

Article

# Scale-Up Strategies of Jet Loop Reactors for the Intensification of Mass Transfer Limited Reactions

Marc Maly<sup>1,\*</sup> , Steffen Schaper<sup>1</sup>, Rafael Kuwertz<sup>2</sup> , Marko Hoffmann<sup>1</sup>, Joachim Heck<sup>2</sup> and Michael Schlüter<sup>1,\*</sup> 

<sup>1</sup> Institute of Multiphase Flows, Hamburg University of Technology, Eißendorfer Str. 38, 21073 Hamburg, Germany

<sup>2</sup> Ehrfeld Mikrotechnik GmbH, Mikroforum Ring 1, 55234 Wendelsheim, Germany

\* Correspondence: marc.maly@tuhh.de (M.M.); michael.schluter@tuhh.de (M.S.); Tel.: +49-40-42878-4331 (M.M.)

**Abstract:** For the purpose of the intensification of an industrial-scale gas-liquid process, the implementation in an alternative reactor concept is investigated at Hamburg University of Technology (TUHH) in cooperation with Ehrfeld Mikrotechnik GmbH. Existing process operation data from a bubble column hint at a mass transfer limitation of the gas-liquid reaction. In the project, a jet loop reactor (JLR) is chosen to increase the specific interfacial area between gas and liquid, and thus increase mass transfer, while keeping the reactor system mechanically simple and low-maintenance. For the investigation, a laboratory scale reactor has been designed on the basis of an existing industrial scale process and scaled according to a pilot scale reactor available at TUHH. For scaling, geometric similarity is desired, while specific energy dissipation rate and volumetric gas input are kept constant for the chosen scale-up strategy. Between the two different scales, the reactors are successfully characterised in a water-air system with regards to the important mass transfer, among other parameters. A pressure- and chemical-resistant twin of the laboratory-scale reactor is provided to the project partner for trials under real process conditions with the original material system. The presented work shows that the JLR concept can be transferred sufficiently well between different scales when suitable parameters are chosen, and offers a wide operating window. The investigations aim to provide a basis for a future scale-up of the chemical process in the JLR system to the industrial scale.

**Keywords:** process intensification; reactor concepts; chemical reactors; scale-up strategies; multiphase flows; mass transfer



**Citation:** Maly, M.; Schaper, S.; Kuwertz, R.; Hoffmann, M.; Heck, J.; Schlüter, M. Scale-Up Strategies of Jet Loop Reactors for the Intensification of Mass Transfer Limited Reactions. *Processes* **2022**, *10*, 1531. <https://doi.org/10.3390/pr10081531>

Academic Editor: Blaž Likozar

Received: 18 July 2022

Accepted: 31 July 2022

Published: 4 August 2022

**Publisher's Note:** MDPI stays neutral with regard to jurisdictional claims in published maps and institutional affiliations.



**Copyright:** © 2022 by the authors. Licensee MDPI, Basel, Switzerland. This article is an open access article distributed under the terms and conditions of the Creative Commons Attribution (CC BY) license (<https://creativecommons.org/licenses/by/4.0/>).

## 1. Introduction

In the context of a cooperative research project between Ehrfeld Mikrotechnik GmbH and the Institute of Multiphase Flows (IMS) at Hamburg University of Technology (TUHH), an existing process for a gas-liquid reaction is to be intensified. So far, a bubble column reactor has been used for the process and data on required gassing rates from operation of the plant hint at a possible mass transfer limitation of the system, limiting the efficiency of the reaction.

In the field of process engineering, a variety of apparatuses are used to provide the required interface for mass transfer between phases, ranging from e.g., simple gassed tanks to bubble columns, stirred tank reactors, and loop reactors [1]. Fast gas-liquid reactions can be critically limited by mass transfer. In these cases, it can be an adequate solution to provide even larger specific interfaces and enhance the mass transfer performance that way. Loop reactors and their derivatives have been proven to be excellent devices for this purpose [1–4]. As such, a jet loop reactor (JLR) is chosen as the tool for the desired process intensification. In the presented implementation of this reactor concept, a concentric draft tube is placed in a tubular reactor. The liquid reactor content is constantly removed at the bottom of the reactor with the help of an external pump, and reinjected in form of a jet at the top via a two-phase nozzle, where the gas phase is added in the center.

Here, the gas phase is intensively dispersed into small bubbles by shear induced by the jet, achieving a large specific interfacial area between the phases [3,5]. A wide range of different (relative) dimensions and designs of nozzles, etc. exist and have been part of scientific investigations for several decades (compare [4,6–17]). Due to its slim design, which results in a relatively low space requirement, and with its external driving mechanism in form of pumps, this reactor type is well suitable to be used for processes requiring elevated pressures, since sealing problems (compared to other mechanical components like stirrers) can be minimised [5,18]. The simplicity of the system also makes it low-maintenance.

As part of the overarching research project, an existing pilot-scale reactor at IMS is scaled down to obtain a laboratory-scale version of the reactor. During scale-down, geometric similarity is desired, while the integral specific energy dissipation rate and volume-specific gas input are kept constant. The system in its different scales is then characterised for a water/air system in regard to mass transfer; the results are presented in this article. In parallel, a pressure- and chemical-resistant twin of the laboratory-scale reactor is created for trials under real process conditions with the original material system on site of the project partner. The project has several aims. Comparative investigations in the laboratory and pilot scale with the model system water/air provide general insight into the scale-up process of the specific jet loop reactor. Further comparative investigations between the laboratory reactors enable studying the effect of the industrial material system. Finally, the laboratory reactor for the industrial material system allows to investigate the applicability of the reactor concept on the existing process of the project partner and provides a basis for further optimisation studies. In Figure 1, a schematic representation of the scaling process is depicted.

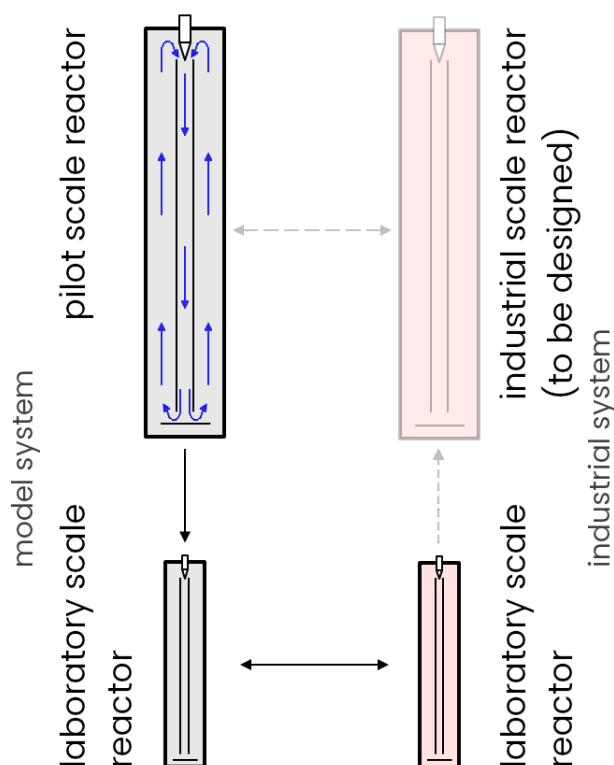


**Figure 1.** Schematic representation of the scale-up; investigations are conducted between the pilot and laboratory scale in the model system water/air (grey), while a comparison between water/air and the industrial system (apricot) is conducted on laboratory scale. The gathered data is used for the scale-up of the chemical process to the industrial scale. Blue arrows exemplarily denote the up- and downwards flow of the loop.

## 2. Materials and Methods

This chapter offers an overview of the reactors used in the research project, and the scale-up process. Furthermore, it provides information on the equipment and methods used for the investigations.

### 2.1. Reactors and Scale-Down

Loop reactors are generally divided into two segments: the riser part, in which the flow is directed upwards, and a down-comer part with the downward flow (refer to blue arrows in Figure 1 for an exemplary depiction). Together, they form a circulating flow, the so-called loop. An internal circulation can be achieved by use of a centrally placed tube. Concepts of jet loop reactors with an external circulation also exist [5]. In the presented research project, a top mounted two-phase nozzle is chosen to introduce the driving momentum of the loop into the system. Following the liquid flow downwards against the direction of buoyancy, and rising in the annular space, the residence time of the introduced gas phase is maximised.

The pilot-scale reactor at IMS is made from flangeable acrylic glass sections, which offer optical access to the processes inside the reactor. A deflection plate is placed above the lower outlet and prevents gas from being sucked into the pump. A centrifugal pump Type CRNE5-8 from Grundfos, Denmark, is used for the pumping of the liquid. The liquid flow rate is measured by a magnetic-inductive flow measuring system of Type Promag 50D from Endress + Hauser, Switzerland. The addition of the gas is measured and controlled by a mass flow controller (MFC) Type FG-201CV from Bronkhorst, Netherlands.

Important dimensions of the pilot-scale setup can be found in Table 1 alongside the dimensions for the laboratory reactor. Photographs of the reactors in both scales are depicted in Figure 2a,b. Schematic implementation of the reactor vessel in the overall setup is depicted in Figure 2c. Figure 3 depicts the nozzle attachment for the laboratory setup.

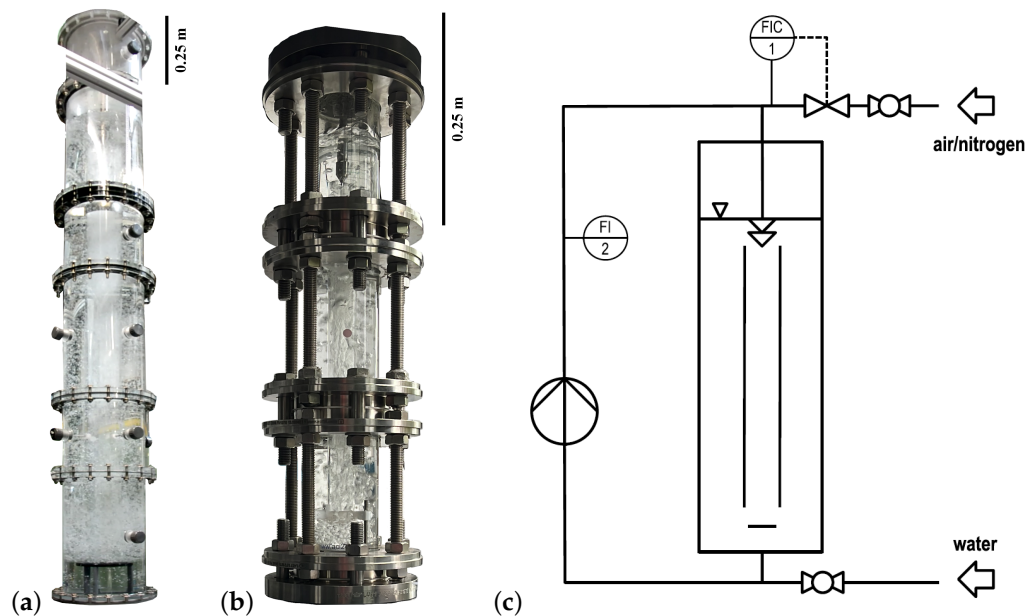


**Figure 2.** Photographs of (a) the pilot scale reactor and (b) the laboratory reactor as used for experiments at IMS and on site of the project partner. (c) Process flow diagram of the setups at IMS.

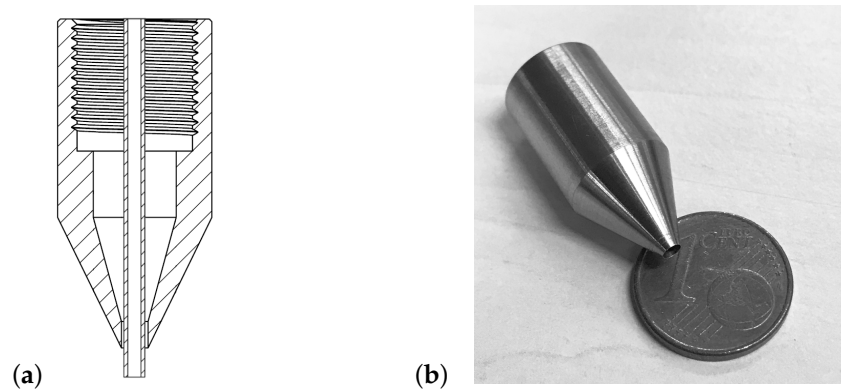


**Figure 3.** (a) Sketch of the scaled nozzle and gas capillary for the laboratory-scale reactor and (b) size of actual nozzle attachment manufactured in 1.4571 by Forschungswerkstatt Maschinenbau (FWM).

**Table 1.** Important dimensions of the reactor setups.

Scale of Reactor:	Pilot	Laboratory
inner diameter of reactor $d_R$ / m	0.288	0.072
filling level $h_O$ / m	1.998	0.499
liquid volume $V_L$ / L	129.0	2.0
inner diameter of draft tube $d_{dt}$ / m	0.096	0.023
length of draft tube $l_{dt}$ / m	1.648	0.412
height of draft tube above bottom $h_{dt}$ / m	0.250	0.063
diameter of deflection plate $d_{dp}$ / m	0.160	0.040
height of deflection plate above bottom $h_{dp}$ / m	0.130	0.033
liquid coverage above nozzle exit $h_c$ / m	0.100	0.025

For the design and manufacturing of the reactors in the laboratory scale, several regulative and/or legal requirements have to be met. Furthermore, two identical systems have to be assembled, one for experiments with a water/air system at IMS, while a chemical- and pressure-resistant twin of the setup is to be provided to the project partner for experiments with the industrial material system under elevated pressures and temperatures. At the same time, the setup should offer optical access like the pilot-scale reactor. For this purpose, pipe sight glasses of Type 620 from ACI Industriearmaturen, Germany, are chosen. The flanges of the reactor version at IMS are manufactured in stainless steel. For the reactor twin of the project partner, the presence of aggressive educts in the experiments requires the use of chemically resistant Hastelloy® C22 for the flange material of the sight glasses and for all other components with direct media contact. The pipe sight glasses are designed for a maximum temperature  $T$  of 200 °C and an operating gauge pressure  $p_g$  of 10 bar(g). The chosen pipe sight glass variant has an inner diameter  $d_{R,L}$  of 0.072 m (listed in Table 1), which leads to a scaling factor

$$\mu = \frac{d_{R,P}}{d_{R,L}} = 4. \quad (1)$$

Any length  $X_i$  of interest is thus scaled according to

$$X_L = \frac{X_P}{\mu} \quad (2)$$

between the scales. Subsequently, the liquid volume  $V_{L,i}$  of the reactors scales according to

$$\mu = \sqrt[3]{\frac{V_{L,P}}{V_{L,L}}} \rightarrow \mu^3 = \frac{V_{L,P}}{V_{L,L}} \quad (3)$$

with a factor  $\mu^3 = 64$ , which results in 2.0 L of liquid volume  $V_{l,L}$  in the laboratory-scale reactor. Three sight glasses are flanged together, resulting in a reactor vessel with a total volume  $V_{t,L}$  of 2.4 L. Additional flanges and internals are manufactured in-house by Forschungswerkstatt Maschinenbau (FWM) of TUHH. To not fall under the requirement of conducting a conformity assessment for pressure vessels as foreseen by the governing legislation in form of the European Pressure Equipment Directive 2014/68/EU, the pressure-volume-product  $p \cdot V$  of the reactor must not reach 25 bar L. Below this point, the design of the vessel is required to be conducted according to good engineering practices. As the basis for this practice, DIN EN 13445 [19] is chosen. The maximum allowed operating pressure  $p_o$  of the system is 8.1 bar with a maximum temperature  $T$  of 200 °C, which still lies above the requirements of the project partner.

Scaling of two-phase contact apparatuses is complicated due to the amount of design parameters and their interactions. Since not all possible quantities can be kept constant or scale differently relative to each other (compare to [20]), a selection of suitable parameters has to be made. In this project, the following aspects are considered in descending order as scale-down criteria:

- a constant volumetric gas input  $\dot{V}_g \cdot V_1^{-1}$
- a constant specific energy dissipation rate  $\epsilon$
- geometric similarity based on the scaling factor  $\mu$
- a constant residence time  $\tau_1$  of the liquid within the reactor.

While other scale-up strategies can focus on constant gas hold-ups, bubble sizes, etc., the constant volumetric gas input  $\dot{V}_g \cdot V_1^{-1}$  is considered in this project. It is of utmost importance for chemical reactions, as it is required to provide the necessary amounts of gaseous educt for the reaction with the liquid phase [20]. Due to the different scaling of volumes and areas and the geometric similarity of the setups, the superficial gas velocities  $u$  for constant volumetric gas inputs are four times larger in the pilot plant than in the laboratory setup (refer to Table 2). During presented investigations, the volumetric gas input is varied to observe the influence of different gassing rates, representing certain stoichiometries, on hydrodynamics.

**Table 2.** Specific gassing rates  $\dot{V}_g$  for experiments in the two setups.

Ratio	$V_1 \cdot \dot{V}_g^{-1} / \text{min}$	34.0	17.0	6.5
<i>setup</i>		gassing rates $\dot{V}_g / \text{L min}^{-1}$		
	<i>pilot scale</i>	3.80	7.60	20.00
	<i>laboratory scale</i>	0.06	0.12	0.31
<i>setup</i>		superficial gas velocity $u / \text{mm s}^{-1}$		
	<i>pilot scale</i>	0.97	1.94	5.12
	<i>laboratory scale</i>	0.25	0.49	1.27

Taking these points into consideration, availability and dimensions of components on the market have to be taken into account as well. For example, the gaseous phase in the laboratory-scale reactor is introduced into the system by a procurable 1/16" capillary. The pumped liquid volume flows are thus modified according to actual implemented geometrical dimensions to achieve same specific energy dissipation rates in both setups. The dimensions of the laboratory setup as given in Table 1 reflect these constraints of part availability.

The integral specific energy dissipation rate  $\epsilon$  has a significant influence on mixing, mass transfer and the interface between the phases in a JLR [21] and is defined as

$$\epsilon = \frac{P}{V_1}, \quad (4)$$

where  $P$  is the power introduced into the system, which is considered to be dissipated in the liquid volume  $V_1$ . The power  $P$  is equalled to the kinetic energy flux  $\dot{E}$ , which is introduced into the system by the pumped liquid [5] and therefore can be described by the pumped liquid mass flow rate  $\dot{m}_f$  and the liquid exit velocity  $w_{n,l}$  of the fluid at the nozzle. Assuming an incompressible fluid, the mass flow rate in turn can be described by the pumped liquid volume flow rate  $\dot{V}_1$  and its density  $\rho_l$ . With these considerations, the specific energy dissipation rate  $\epsilon$  can be expressed as

$$\epsilon = \frac{P}{V_1} = \frac{\dot{E}}{V_1} = \frac{\frac{1}{2}\dot{m}_f \cdot w_{n,l}^2}{V_1} = \frac{\frac{1}{2}\dot{V}_1 \cdot \rho_l \cdot w_{n,l}^2}{V_1}. \quad (5)$$

The nozzle exit velocity  $w_{n,l}$  of the fluid can be calculated with knowledge of the pumped liquid volume flow rate  $\dot{V}_1$  and the nozzle exit area  $A_{n,l}$  for the fluid according to

$$w_{n,l} = \frac{\dot{V}_1}{A_{n,l}}. \quad (6)$$

The nozzle exit velocity  $w_{n,g}$  of the gas is similarly calculated as

$$w_{n,g} = \frac{\dot{V}_g}{A_{n,g}} \quad (7)$$

with the gas volume flow rate  $\dot{V}_g$  and its nozzle exit area  $A_{n,g}$ . Technically, the contribution of the gaseous phase to energy input has to be taken into consideration too, but due to the low density  $\rho_g$  of the gaseous phase, even at pressures of intended future operation, it can be considered negligible in the context of this project. The contribution to energy input for volumetric gassing rates taken from the process amount to less than 0.13%.

An example for a quantity that can not be kept constant under the agreed-upon scaling parameters of this work is the Reynolds number  $Re$  of the jet, defined as

$$Re = \frac{\rho_l \cdot w \cdot l}{\eta} = \frac{\rho \cdot w_{n,l} \cdot d_h}{\eta} \quad (8)$$

within this work, with the hydraulic diameter  $d_h$  of the nozzle gap as the characteristic length  $l$  [22]. As the density  $\rho_l$  and viscosity  $\eta_l$  of the liquid remain the same and the nozzle exit velocity  $w_{n,l}$  is in a similar order for both setups, the difference in hydraulic diameter  $d_h$  leads to a factor of about 11.6 between the Reynolds numbers in the pilot scale ( $Re_{n,p}$  in order of  $10^3$ ) and the laboratory scale ( $Re_{n,L}$  in order of  $10^4$ ), similar to the difference in the scale-down investigations of Wiedemann [4,21].

To scale the feed volume flow rate  $\dot{V}_e$  of the liquid educt in relation to the reactor content  $V_1$ , a constant residence time of the liquid

$$\tau_1 = \frac{V_1}{\dot{V}_e} \quad (9)$$

is used. Data from the existing process is taken as a basis. For experiments on site of the project partner, fresh educt is added to the circulating volume flow. For experiments at IMS, this addition and discharge is not considered as it is not required in the water/air system. However, as the aim of the project is the intensification of the existing process, the residence time  $\tau_1$  under overstoichiometric gassing is to be reduced by increasing liquid throughput of the system. For further intensification, the gas flow rate  $\dot{V}_g$  is to be increased and the residence time  $\tau_1$  further decreased to benefit from the advantages offered by the jet loop reactor.

In the scaled laboratory setup, a gear pump from Ismatec, Switzerland, of Type MCP-Z Standard with a pump head of Type Z-140 P with a maximum pumping flow rate of  $3.84 \text{ L min}^{-1}$  and a maximum differential pressure of 5.6 bar is used. A magnetic-inductive flow meter from ifm electronic, Germany, Type SM6050, can be used to measure the pumped

liquid flow. The gas volume flow is controlled by another mass flow controller Type F-201CV from Bronkhorst, Netherlands. The internals (deflection plate, draft tube holders) are made from PTFE, which is stable under process conditions.

## 2.2. Media

For experiments at IMS, the reactors are operated with demineralised water and pressurised air. The electric conductivity  $\sigma$  of the demineralised water at IMS varies between 3 and 5  $\mu\text{S cm}^{-1}$ . Since the magnetic-inductive flow meters in both setups require a minimum electric conductivity  $\sigma$  of 20  $\mu\text{S cm}^{-1}$  in the liquid, the liquid conductivity has to be increased. For this reason, sodium chloride (NaCl) is added to and thoroughly mixed with the reactor content, setting a concentration  $c_s$  of 15  $\text{mg L}^{-1}$ . This salt concentration increases the conductivity by 30  $\mu\text{S cm}^{-1}$  [23] and thus above the required minimum level. Nitrogen and pressurised air are used during experiments as the gaseous phase.

## 2.3. Parameters of Investigation

The used, scaled gassing rates  $\dot{V}_g$  are listed in Table 2. The vessel is unpressurised for the experiments; gas flows are given under operating conditions. The ratio  $V_1 \cdot \dot{V}_g^{-1}$  between gassing rate  $\dot{V}_g$  and reaction volume  $V_1$  is kept constant between the scales and used to compare measurements between the setups. The ratio  $V_1 \cdot \dot{V}_g^{-1}$  is the reciprocal of VVM (vessel volumes per minute, as commonly used in bioprocess engineering); a lower value means a higher gassing rate in relation to the reactor content. During the experiments, different specific energy dissipation rates  $\epsilon$  are applied to the systems. The different liquid volume flow rates  $\dot{V}_l$  which are required to achieve the chosen specific energy dissipation rates  $\epsilon$  in the two setups are listed in Table 3.

**Table 3.** Investigated specific energy dissipation rates  $\epsilon$  and scaled liquid volume flow rates  $\dot{V}_l$  of water in the pilot- and laboratory-scale plants.

spec. Energy Dissipation Rate $\epsilon / \text{kW m}^{-3}$	1.02	1.50	2.03	2.63	3.29	4.00
<i>setup</i>	corresponding volume flow rates $\dot{V}_l / \text{L min}^{-1}$					
<i>pilot scale</i>	47.93	54.49	60.32	65.67	70.83	75.61
<i>laboratory scale</i>	1.06	1.20	1.33	1.45	1.56	1.67

## 2.4. Investigation Methods

The following subsections explain the methods used in the investigation of different phenomena. The data gathered with the help of these investigation methods in conjunction with the experiments on site of the project partner is the basis for comparisons between the different scales of the reactor and for the future scale-up.

### 2.4.1. Determination of Bubble Sizes

Digital image evaluation is used for the analysis of the bubble size distributions in this work. As photo quality plays an important role in image evaluation, an LED panel and a high-resolution camera are required to obtain clear bubble contours in the images. The LED panel is installed opposite the camera to provide a homogeneous background illumination. A Nikon D7500 is used as the camera for the photos taken at the pilot plant scale, and a Nikon D7100 for the photos taken at laboratory scale. In both cases, a 50 mm lens (Planar T\* 2/50 ZM from Zeiss, Germany) with a shallow depth of focus is used. For a determination of the ratio between pixels and millimeters, known lengths are required. In the pilot scale, markings for lengths of 20 mm are added to the inside of the reactor wall and the outside of the draft tube in the observation window. For the laboratory scale reactor, the known outer diameter of the draft tube and the known diameter of a probe spot are available for calibration. During image recording, the focus plane is set in the annular space and evaluation of bubbles is focused on the sharp focus plane and the middle section of the reactor, where distortions of the curved surface are minimal. To reduce optical

distortions in both setups further, aquariums are placed around the reactors for the purpose of refractive index matching, which are filled with demineralised water. Figure 4 shows the setup in the pilot scale with the octagonal aquarium.

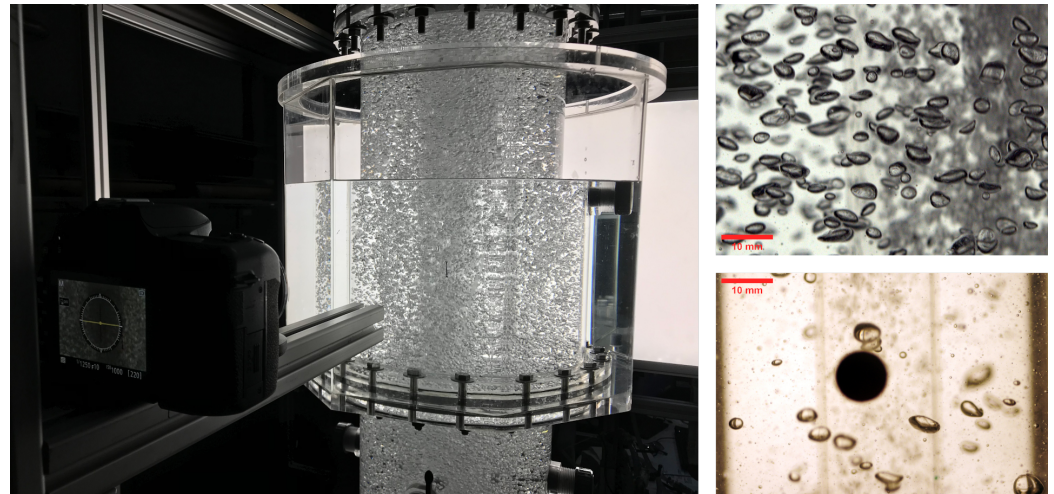


**Figure 4.** (Left side): Pilot-scale reactor with the installed aquarium for refractive index matching; the camera is in the foreground, while the LED panel, which provides a homogeneous background illumination, is located on the opposite side. (Right side): exemplary photos of bubble collectives for  $V_1 \cdot \dot{V}_g^{-1} = 17.0 \text{ min}$  and  $\epsilon = 4.0 \text{ kW m}^{-3}$  in the pilot (top) and laboratory reactor (bottom).

The recorded ellipsoid bubbles in the focus plane are evaluated by hand with the help of the open source software ImageJ to obtain their minor and major diameters,  $d_{mi}$  and  $d_{ma}$  respectively. Surface area  $A$  and volume  $V$  of each bubble are calculated as described in Appendix A. For a collective of  $n$  bubbles, the Sauter mean diameter

$$d_{32} = 6 \cdot \frac{\sum_{i=1}^n V_i}{\sum_{i=1}^n A_i} \quad (10)$$

can be determined to compare different bubble collectives [24]. The comparison of bubble sizes in this work is based on Sauter mean diameters.

#### 2.4.2. Determination of Gas Hold-Up

The global gas hold-up is determined by measuring the filling level  $h$  of the aerated liquid in relation to the unaerated filling level  $h_0$ . The pump is operated during both determinations. With the help of  $h$ , the gas volume  $V_g$  in the reactor liquid can be determined and set into relation to the unaerated liquid volume  $V_l$  to obtain the gas hold-up

$$\epsilon_g = \frac{V_g}{V_l + V_g}. \quad (11)$$

The volume of the internals is taken into account in the determination. As the gassing rate increases, the precision in determining the liquid level height  $h$  decreases due to the unstable, moving liquid surface. Triplicate measurements are taken for each determination at points in time at which the surface moves the least. It has to be noted that the read-off accuracy ( $\pm 0.5 \text{ mm}$ ) can lead to a relatively high error for very low gas hold-ups (up to 25% for the minimum reading of 2.0 mm).

### 2.4.3. Determination of Volumetric Mass Transfer Coefficient

For the determination of the volumetric mass transfer coefficient  $k_L a$ , the dynamic method is used. For this, the nitrogen-stripped system is gassed with air and the increase in dissolved oxygen concentration  $c$  is measured over time. The volumetric mass transfer coefficient  $k_L a$  can be calculated with the help of

$$\frac{dc}{dt} = k_L a \cdot (c^* - c(t)), \quad (12)$$

for which the saturation concentration  $c^*$  of the system has to be known [25]. The saturation concentrations are measured for the different operating points in the different systems by gassing with air until a constant concentration is reached. For each measurement, the system is stripped with nitrogen first to bring the oxygen saturation below 15%. For the determination of the volumetric mass transfer coefficient  $k_L a$ , the stable slope of the linear regression of the logarithmic dissolved oxygen concentration difference

$$\ln \frac{c^* - c(t)}{c^* - c_0} = -k_L a \cdot (t - t_0). \quad (13)$$

is evaluated between 20% and 80% when gassed with air. All measurements are conducted in triplets. In the pilot scale, a dissolved oxygen sensor FDO 925 from WTW, Germany, is used for the measurements and installed at half of the filling height of the reactor (response time  $t_{90}$  of the probe below 30 s). Because the probe is too large for the laboratory scale reactor and would significantly influence the hydrodynamics of the system, the measurements in this system are undertaken with non-invasive oxygen sensor spots of Type SP-PSt3 ( $t_{90} < 40$  s) from PreSens Precision Sensing, Germany, in conjunction with a compact fiber optic oxygen meter PreSens OXY-1 SMA.

### 2.4.4. Determination of the Stability of the Loop

The stability of the loop is simply quantified as ‘stable’ or ‘unstable’. To determine the stability of the loop, the reactor is operated with a desired pumped liquid flow rate  $\dot{V}_l$ . Then the gassing is started. Subsequently, the gassing rate  $\dot{V}_g$  is increased step by step every two minutes to find the combination of liquid flow rate  $\dot{V}_l$  and maximum gassing rate  $\dot{V}_{g,max}$  at which the loop breaks down. The determination of the point of break-down is conducted several times to obtain valid, replicable results.

## 3. Results

In the following subsections, the different results of the characterisation measurements between the two scales are presented and discussed.

### 3.1. Bubble Sizes

Gathered Sauter mean diameters  $d_{32}$  for the recorded bubble collectives in the pilot and laboratory setups for different specific gassing rates and specific energy dissipation rates are shown in Figure 5.

For the pilot setup, the influence of the specific energy dissipation rate and the gas input on the Sauter mean diameter is directly recognisable. It can be seen that an increase in the power input leads to a slight but steady reduction in the Sauter mean diameter, as is to be expected. Increasing the specific energy dissipation rate in the reactor leads to an increase in turbulence and shear effects, and thus, while keeping the gas addition constant, an increased break up of gas bubbles. An increase in the gas volume flow rate on the other hand, while keeping the specific energy dissipation rate constant, leads to increased coalescence as well as a distribution of the dissipation effect over a larger amount of gas and thus is reflected in an increase in Sauter mean diameters. Depending on the specific energy dissipation rate and the gas volume flow rate, Sauter mean diameters are in the range of 3.1 to 4.3 mm. On average, 240 bubbles have been evaluated by hand for each data point. The bubble collectives (exemplarily depicted in Figure 4, top right) are very

homogeneous. They mainly consist of ellipsoidal bubbles of similar size, with only few spherical bubbles below 1 mm in diameter, which have no significant effect on the Sauter mean diameter.

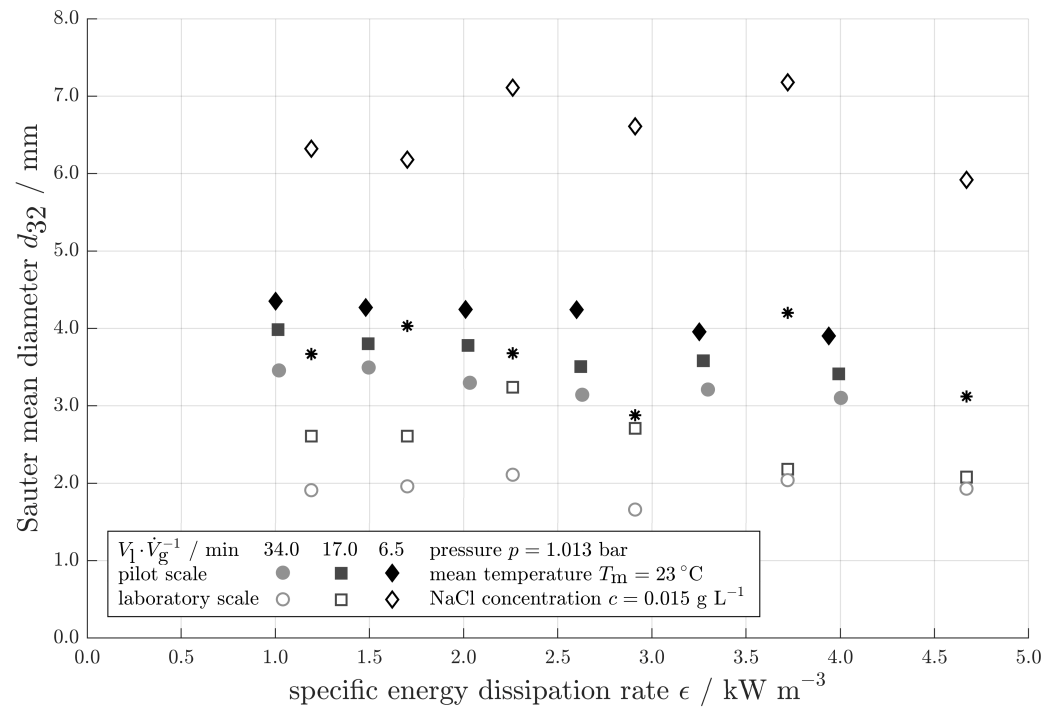


**Figure 5.** Sauter mean diameters  $d_{32}$  in the pilot and laboratory setups for different specific gasing rates  $V_1 \cdot \dot{V}_g^{-1}$  and specific energy dissipation rates  $\epsilon$ . Asterisks (\*) denote data points obtained for the highest gasing rate in the laboratory setup from which outliers due to coalescence have been eliminated.

In the laboratory scale, the Sauter mean diameters show values in the range of 1.66 to 7.18 mm. For each data point, on average 385 bubbles have been evaluated by hand. Overall, for same ratios of  $V_1 \cdot \dot{V}_g^{-1}$  and specific energy dissipation rates, Sauter mean diameters are of a similar order of magnitude in both setups. Nevertheless, the Sauter mean diameters for the high gasing rate in the laboratory system differ significantly by exhibiting much larger values. These discrepancies can be explained by the bubble collectives. In the laboratory setup, significantly different distributions form compared to the pilot setup. Here, small, spherical bubbles with diameters below 1 mm dominate, while comparatively few large ellipsoidal bubbles are present (exemplarily depicted in Figure 4, bottom right). The size of these larger, ellipsoidal bubbles is in the same range as for the bubbles found in the pilot plant. These bubbles dominate the overall Sauter mean diameter due to how it is calculated. Some of these ellipsoidal bubbles coalesce into especially large bubbles, which significantly influence the Sauter mean diameter and result in the aforementioned discrepancies. When these coalesced bubbles are taken out of the data sets for the high gasing rate (0.7% of evaluated bubbles of said data set), the resulting Sauter mean diameters would be between 2.9 and 4.2 mm. This shows again the importance of taking underlying bubble collectives into consideration when comparing bubble sizes based on Sauter mean diameters. For comparison purposes, the modified Sauter mean diameters  $d_{32^*}$  marked as asterisks in Figure 5 show the obtained values for the data obtained for the highest gasing rate in the laboratory setup after these 0.7% of outliers have been eliminated.

In an explanation of this differing behaviour, the difference in scaling of volumes and surfaces has to be considered. The ratio of the volume in the draft tube to its internal surface differs by a factor of 4 between the setups, with the laboratory system specifically showing a

relatively larger wall surface. Thus, possible wall effects/interactions are more pronounced here. Furthermore, the materials are different; in the pilot reactor, acrylic glass is used, while borosilicate glass and PTFE holders are used in the lab reactor. The differences between these materials (surface roughnesses, surface tensions) can have an influence on the gaseous phase, its coalescing behaviour and thus the Sauter mean diameters. Also, the area between the insertion tube and the deflection plate, which has to be passed by bubbles, differs relatively and represents a constriction for the bubbles in the laboratory system, which can lead to increased coalescence. Furthermore, the integral specific energy dissipation rate, which causes the shear responsible for the formation of the initial bubble collective in the jet, is an integral quantity and its manifestation (locally, temporally, and in absolute size) can vary. Another important factor is the formation of the bubbles at the nozzle exit itself. This can be characterised by the Weber number  $We$ . In the current form of the setups, the Weber number varies significantly for different operating points in one setup, but also between the setups themselves due to the geometrical scaling. To reach more similar bubble size distributions, a scaling approach based on these parameters is possible, but requires constructional measures. Alternatively, the gas flow rates can be changed to achieve equal superficial gas velocities, as often recommended in scale-up investigations. This would entail a change in the liquid educt addition to suit the industrial reaction, and thus a significant change of the residence time of the liquid in the reactor.

### 3.2. Gas Hold-Up

The gas hold-ups  $\epsilon_g$  in the pilot plant reactor and the laboratory setup are depicted in Figure 6 in relation to the specific energy dissipation rate  $\epsilon$  for the different gas inputs  $\dot{V}_g^{-1}$  per reaction volume  $V_l$ . Bars show the standard deviation of the measurements conducted in triplicates.

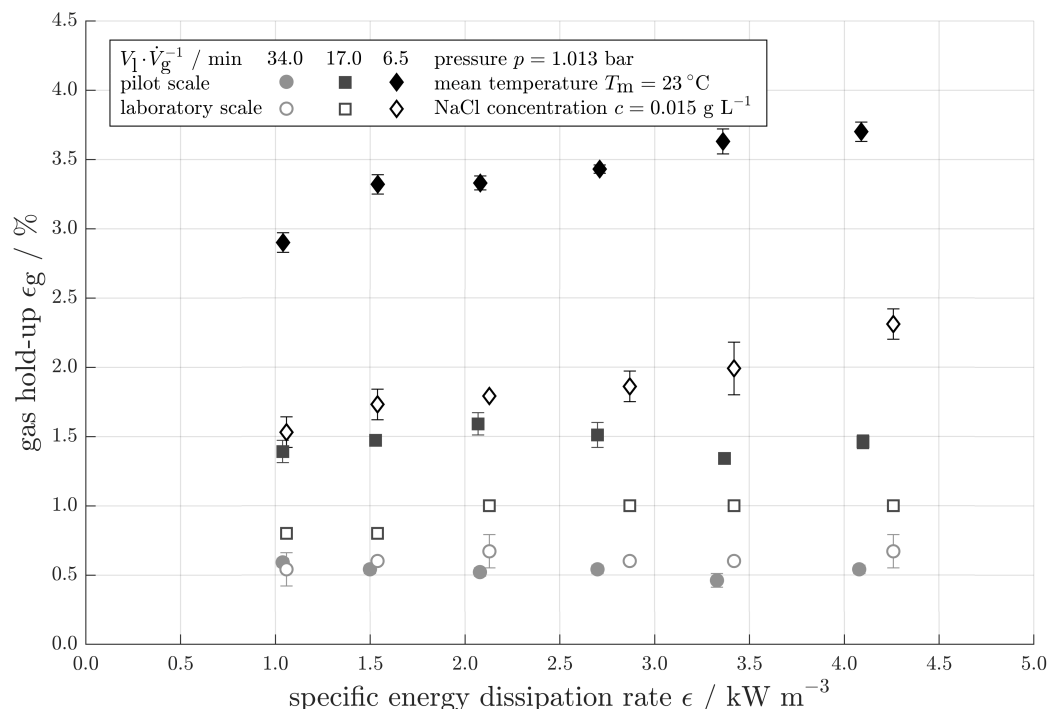


**Figure 6.** Gas hold-up  $\epsilon_g$  in relation to the specific energy dissipation rate  $\epsilon$  in both the pilot- and laboratory-scale setup.

For higher specific gassing rates, as expected, the gas hold-up increases with increasing specific energy dissipation rate. The gas phase tends to be dissipated more strongly into bubbles with smaller diameters with increasing specific energy dissipation rate. These smaller bubbles remain longer in the system, as their reduced buoyancy leads them to follow

the liquid flow more easily, while at the same time the stronger loop flow in these cases increases the circulating gas hold-up even further. At lower specific gassing rates however, the gas content appears to be almost independent of the specific energy dissipation rate.

For a better comparison of the gas hold-up in the two setups, a dimensionless group is desired. For this group, the following parameters are chosen: The specific energy dissipation rate  $\epsilon$  as a measure for the energy input into the system, the ratio between the nozzle exit velocities of the gas and the liquid,  $w_{n,g}$  and  $w_{n,l}$ , respectively; furthermore, the relation between gassing rate  $\dot{V}_g$  and the liquid content  $V_l$  of the reactor. For de-dimensioning of the group, the density  $\rho_l$  of the liquid and the gravitational constant  $g$  are used. These parameters are arranged to form a dimensionless group  $\epsilon \cdot w_{n,g} \cdot w_{n,l}^{-1} \cdot \dot{V}_g \cdot V_l^{-1} \cdot \rho_l^{-1} \cdot g^{-2}$ . With the help of this group, an empirical correlation is derived to predict the gas hold-up according to

$$\epsilon_g = 0.51 \cdot (\epsilon \cdot w_{n,g} \cdot w_{n,l}^{-1} \cdot \dot{V}_g \cdot V_l^{-1} \cdot \rho_l^{-1} \cdot g^{-2})^{\frac{1}{3}}. \quad (14)$$

A log-log plot of all recorded gas hold-ups in relation to the dimensionless group, together with the empirical correlation, is depicted in Figure 7.

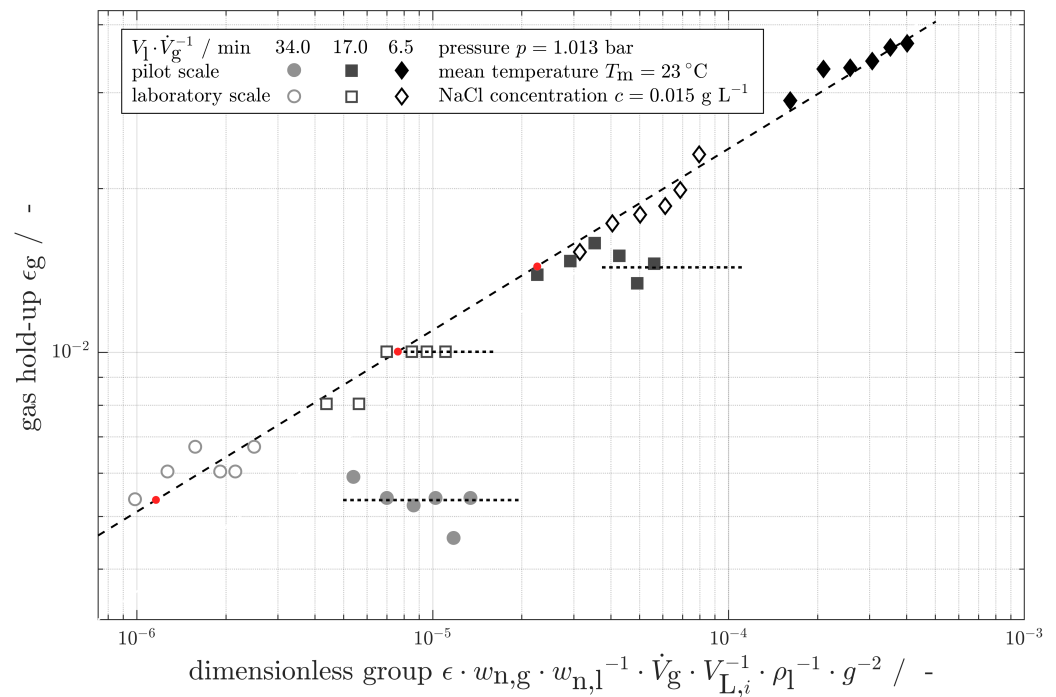


**Figure 7.** Recorded gas hold-ups  $\epsilon_g$  for both systems in dependence of the formulated dimensionless group  $\epsilon \cdot w_{n,g} \cdot w_{n,l}^{-1} \cdot \dot{V}_g \cdot V_l^{-1} \cdot \rho_l^{-1} \cdot g^{-2}$ . Also plotted is the correlation based on the dimensionless group (Equation (14)). Transition points to saturated states marked as red points.

It can be seen that the measured values for the gas hold-up mostly follow the correlation sufficiently well, but also that for some sets of gassing rates and specific energy dissipation rates, they seem to reach a transition point. After reaching this point, a further increase in specific energy dissipation rate does not result in any significant change of the gas hold-up in comparison to the error of the read-off accuracy. Nonetheless, the deviation to the plotted correlation is significant and far larger than the errors springing from inaccuracies from read-off. Here it is understood that the specific energy dissipation rate is at some point sufficient enough to finely disperse the added gas phase, without any further potential of breaking the gas phase into even finer bubbles or retaining more gas in the loop. At this point, the gas hold-up reaches a steady “saturated” level, and thus, for a constant gassing rate, cannot be increased further with an increase in specific energy

dissipation rate. Rosseburg et al. have reported a similar phenomenon, but in stirred tank reactors. There, a steadily increasing gas hold-up for increasing Froude numbers was found, until a saturation value was reached and after that point, marked by a homogeneous, well distributed bubbly flow, the gas hold-up stayed constant as well (compare to [26]). In the presented case, the coefficient of determination of the correlation lies at  $R^2 = 0.9459$  for recorded data, excluding the constant values in gas hold-up (see horizontal lines in Figure 7). Outside the scope of the research project, a broader data basis is needed to verify the model and determine the boundaries of applicability, e.g., prediction of possible transition points.

### 3.3. Volumetric Mass Transfer Coefficient

Figure 8 shows the determined volumetric mass transfer coefficients in both setups. The volumetric mass transfer coefficients in the pilot-scale plant range from  $k_{L}a = 18.0 \text{ h}^{-1}$  to  $93.6 \text{ h}^{-1}$ , depending on the specific energy dissipation rate and the gassing rate. In the laboratory setup, the volumetric mass transfer coefficients exhibit values between  $23.3 \text{ h}^{-1}$  and  $91.1 \text{ h}^{-1}$ .

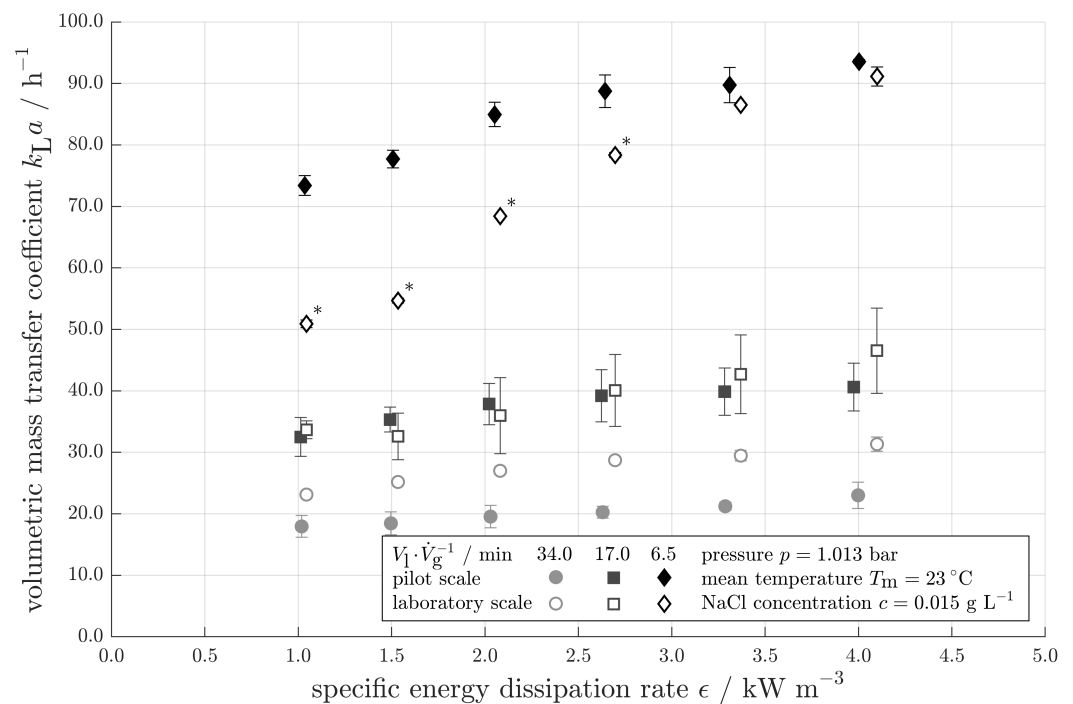


**Figure 8.** Comparison of determined volumetric mass transfer coefficients  $k_{L}a$  in the pilot and laboratory setup for different gassing rates  $V_1 \cdot \dot{V}_g^{-1}$  at investigated specific energy dissipation rates  $\epsilon$ . An asterisk (\*) next to a data point denotes increased coalescence.

The results show, as expected, that the volumetric mass transfer coefficients are influenced by the gassing rate and the specific energy dissipation rate and increase with an increase in either of these two parameters. This effect is more pronounced with the higher gas volume flow rates than with the lower ones. It is likely that the increasing gas hold-up and increasing interfacial area with increasing specific energy dissipation rate can be cited as a reason for this. For the lower gassing rates, the gas hold-up remains approximately constant with increasing energy dissipation, as shown before. With increasing specific energy dissipation rate, the decrease in Sauter mean diameter takes place in the same order of magnitude as for all gassing rates, as shown before. With the combination of an increase in gas hold-up and a simultaneous decrease in Sauter mean diameter, the specific interfacial area increases more strongly for the highest specific gassing rates. For the lower specific gassing rates, the increase in the specific phase interface is only due to the decrease in bubble size.

The volumetric mass transfer coefficients in the laboratory scale are of the same order of magnitude as those determined in the pilot plant scale, especially for the two lower gassing rates. At the highest specific gassing rate however, they differ significantly for lower specific energy dissipation rates between the scales, with the volumetric mass transfer coefficients being lower in the laboratory setup. The lower values can be explained by the occurrence of larger bubbles in the insertion tube, caused by an increased coalescence. The larger bubbles lead to a decrease in the specific interfacial area between the phases and thus also to a decrease in the volumetric mass transfer coefficient. With increasing specific energy dissipation rate, the gas phase is more easily and finely dispersed, and as such the values for the volumetric mass transfer coefficients start to converge on similar levels.

The volumetric mass transfer coefficient is an integral parameter which is decisively influenced by a variety of parameters such as the gas hold-up, the bubble size distribution, the specific energy dissipation rate and the hydrodynamics of the system. Due to it being an integral quantity, statements about the influence of the scale-down on local processes can not be made [4,21]. However, the relatively good agreement of measured values in both scales presented in this work shows that under geometric similarity of the setups, the utilisation of the specific energy dissipation rate and the volume-specific gas input have been purposeful in the desired scale-up.

### 3.4. Stability of the Loop

The pilot and the laboratory plant both show a steady increase of maximum achievable gassing rates with increasing specific energy dissipation rates in the investigated range. For a direct comparison of the setups, the maximum achievable gassing rates are set into relation to the liquid reactor content in form of  $V_1 \cdot \dot{V}_{g,\max}^{-1}$ . The comparison is depicted in Figure 9.

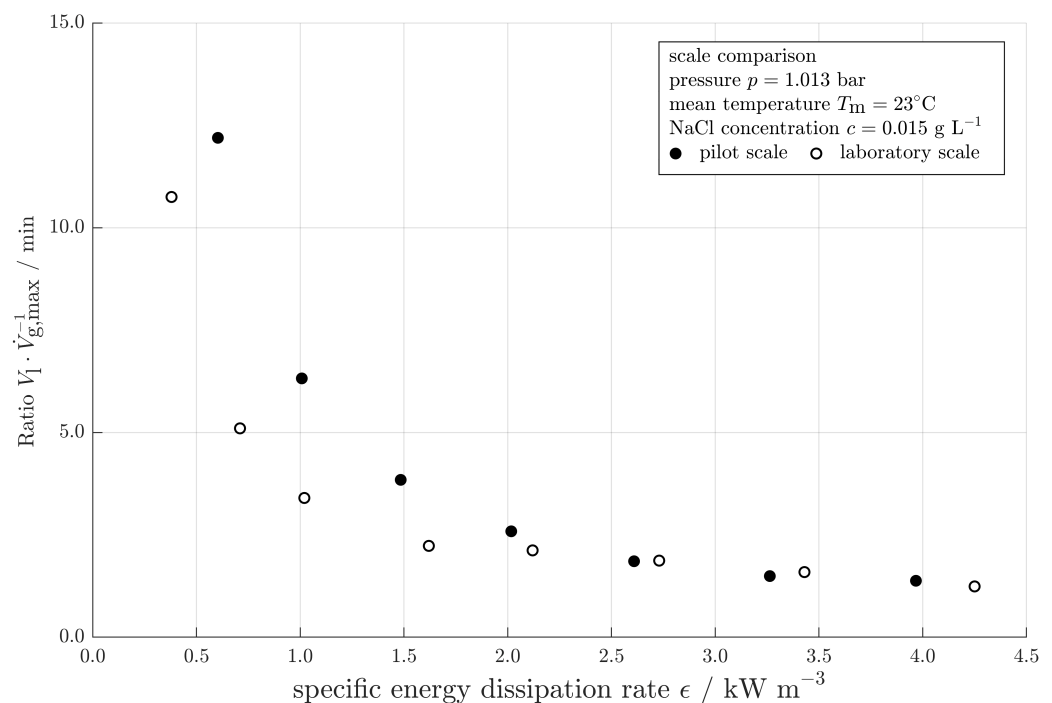


**Figure 9.** Comparison of the maximum achievable gassing rates  $\dot{V}_{g,\max}$  in form of the ratio  $V_1 \cdot \dot{V}_{g,\max}^{-1}$  for the two investigated scales of the reactor for different specific energy dissipation rates  $\epsilon$ .

Both systems show a quite similar behaviour, with deviations for lower specific energy dissipation rates. Here, the laboratory system can form a stable loop for relatively higher gas volume flow rates. This seems curious at first, when it is taken into account that bubble sizes for high gassing rates are in similar ranges (except for coalesced outliers). But the

improved stability is ascribed to exactly this fact. Since bubble sizes do not scale in the same way as the geometry of the setups, part of the bubbles in the laboratory system are relatively larger in relation to the setup dimensions (also compare to Figure 4). In general, the liquid jet at the nozzle pulls a certain share of rising bubbles from the annular space into the insertion tube. The relatively larger bubbles in the laboratory system are less prone to be affected by this than the existing smaller bubbles, and leave the liquid via the head space of the reactor. This is also reflected in the gas hold-ups, which are significantly lower in the laboratory system compared to the pilot system (see Figure 6). As a result, less energy is needed to circulate this reintroduced gas phase and it is instead available to contribute to the stability of the system. With increasing specific energy dissipation rate, bubbles are sheared more, the smaller bubbles are kept more in the system, and the behaviour of the systems exhibits a more similar behaviour.

#### 4. Discussion

Presented within this work is the scale-up, design and characterisation of a jet loop reactor for the investigation of the intensification of a process with a mass transfer limitation. For the implementation of the existing process in the future industrial scale and the required scale-up, investigations are conducted in pilot and laboratory scale. The chosen parameters of geometric similarity of the reactor setups, a constant volumetric gas input, and a constant specific energy dissipation rate have proven purposeful in the creation of sufficiently similarly performing reactors in the two scales when it comes to the desired operating window of the project partner, especially in regard to the mass transfer.

An empiric correlation was formulated for the prediction of gas hold-ups up to a saturation level in the presented system. This correlation requires further experiments to investigate its applicability in other jet loop reactor setups and especially other material systems; the influences of surface tension and viscosity should unarguably play a role in the occurring gas hold-up, but are not represented in the current correlation. Furthermore, the prediction of saturation levels is required to find the limits of the correlation.

Overall, the presented work shows that the JLR-concept can be transferred well between different scales when suitable parameters are chosen. A key parameter here is the specific energy dissipation rate, which can easily be manipulated by changing pumped liquid volume flow rates. With simple changes in the integral specific energy dissipation rate, a broad and flexible operating window can be used for processes. The findings have now to be combined with future experiments with the industrial material system to provide a profound basis for the future scale-up.

#### 5. Outlook

Systematic series of experiments with the industrial material system are to be conducted on site of the project partner with the provided pressure- and chemical-resistant twin of the reactor setup (see Figure 10). The original material system shows a greatly different surface tension and viscosity, which has to be investigated. With regard to the intended use of organics, the surface tension is significantly reduced, which leads to smaller, more homogeneous bubbles, thus higher specific surfaces and even higher mass transfer coefficients, compared to the investigated water/air system presented here. The observed coalescence and its resulting effects are expected to be reduced significantly in the organic system.

Before shipping, the setup for the project partner has been characterised with water and air to ensure sufficiently similar performance between the twin reactors. On site of the project partner, first experiments have already shown the applicability of the JLR-concept to the process and resulted in an efficient use of the reaction gas in batch operation, resulting in a decrease of required residence times.

With systematic series, the hydrodynamics (e.g., pressure losses over the nozzle, stability of the loop with varying gassing rates and specific energy dissipation rates) of the reactor with the original system are to be investigated to gather necessary information for the scale-up. Meanwhile, the operating parameters are further tweaked and optimised in

other experiments with regard to an increased space-time yield. Final target is the scale-up of the reactor system to achieve continuous operation on industrial scale.



**Figure 10.** Completely assembled and equipped setup for experiments with the original material system on site of the project partner.

**Author Contributions:** Conceptualization, M.M., R.K. and M.S.; methodology, M.M.; validation, S.S.; formal analysis, S.S. and M.M.; investigation, S.S. and M.M.; resources, M.H., R.K. and M.S.; writing—original draft preparation, M.M.; writing—review and editing, S.S., R.K., M.H., J.H. and M.S.; visualization, M.M.; supervision, M.S. and R.K.; project administration, M.M.; funding acquisition, R.K. and J.H. All authors have read and agreed to the published version of the manuscript.

**Funding:** This research was funded by Ehrfeld Mikrotechnik GmbH in the scope of a cooperative industrial research project.

**Acknowledgments:** The authors would like to thank the staff of Forschungswerkstatt Maschinenbau at TUHH and our very own technician at the institute, Bernhard Pallaks, for their continued, skilled support in the manufacturing of setup components. For the discussion of questions arising from the correct application of DIN EN 13445 during the design of the laboratory-scale reactor, the authors want to gratefully thank Fernando Lidonnici, Chairman and Treasurer of the European Pressure Equipment Research Council, and Arne Pietsch, Technische Hochschule Lüneburg. Special thanks is given to our student Anahita Radmehr, who worked tirelessly with us for the timely assembly of the reactors. Many thanks for the discussion and help during the refinement process of the correlation for the gas hold-up are due to Jürgen Fitschen.

**Conflicts of Interest:** The authors declare no conflict of interest.

## Abbreviations

The following abbreviations are used in this manuscript:

FWM	Fachwerkstatt Maschinenbau
IMS	Institute of Multiphase Flows
JLR	Jet Loop Reactor
LED	Light-Emitting Diode
MFC	Mass Flow Controller
NaCl	sodium chloride
PTFE	Polytetrafluoroethylene
TUHH	Hamburg University of Technology
VVM	vessel volumes per minute

## Appendix A. Bubble Calculations

For the calculation of the surface area  $A$  and volume  $V$  of completely spherical bubbles, with minor  $d_{mi}$  and major  $d_{ma}$  being equal, the formulas

$$A = 4 \cdot \pi \cdot \frac{d^2}{2} \quad (\text{A1})$$

and

$$V = \frac{\pi}{6} \cdot d^3 \quad (\text{A2})$$

for spheres apply. All other bubbles are considered as oblate spheres and as such the surface area  $A$  is calculated according to

$$A = 2 \cdot \pi \cdot d_{ma}^2 \cdot \left[ 1 + \frac{d_{mi}^2 \cdot \operatorname{artanh}(e)}{e \cdot d_{ma}^2} \right], \quad (\text{A3})$$

with the numerical eccentricity

$$e = \sqrt{1 - \left( \frac{d_{mi}}{d_{ma}} \right)^2}, \quad (\text{A4})$$

while the volume is calculated according to

$$V = \frac{4}{3} \pi \cdot d_{ma}^2 \cdot d_{mi}. \quad (\text{A5})$$

## References

- Lohrengel, B. Untersuchungen zur Fluidodynamik zwei- und dreiphasig betriebener Schlaufenreaktoren. Ph.D. Thesis, Technische Universität Clausthal, Clausthal, Germany, 1990.
- Behr, A.; Becker, M. Multiphase Catalysis in Jetloop-Reactors. *Chem. Eng. Trans.* **2009**, *17*, 141–144. [[CrossRef](#)]
- Behr, A.; Becker, M.; Dostal, J. Bubble-size distributions and interfacial areas in a jetloop reactor for multiphase catalysis. *Chem. Eng. Sci.* **2009**, *64*, 2934–2940. [[CrossRef](#)]
- Wiedemann, M.; Rübiger, N.; Schlüter, M.; Eisenlauer, J.; Riener, F.X.; Kutschera, D.; Neumann, S. Scale-down des Strahlzonen-Schlaufenreaktors: Entwicklung eines Screening-Tools für transportlimitierte chemische Reaktionen. *Chem. Ing. Tech.* **2010**, *83*, 349–357. [[CrossRef](#)]
- Schlüter, M.; Warnecke, H.J.; Zehner, P. Reaktoren für Fluid-Fluid-Reaktionen: Schlaufenreaktoren. In *Handbuch Chemische Reaktoren: Grundlagen und Anwendungen der Chemischen Reaktionstechnik*; Reschetilowski, W., Ed.; Springer: Berlin/Heidelberg, Germany, 2019; pp. 1–32. [[CrossRef](#)]
- Blenke, H.; Bohner, K.; Schuster, S. Beitrag zur optimalen Gestaltung chemischer Reaktoren. *Chem. Ing. Tech.* **1965**, *37*, 289–294. [[CrossRef](#)]
- Blenke, H.; Bohner, K.; Pfeiffer, W. Hydrodynamische Berechnung von Schlaufenreaktoren für Einphasensysteme. *Chem. Ing. Tech.* **1971**, *43*, 10–17. [[CrossRef](#)]
- Zehner, P. Suspendieren von Feststoffen im Strahlschlaufenreaktor. *Chem. Ing. Tech.* **1980**, *52*, 910–911. [[CrossRef](#)]

9. Tebel, K.H.; Zehner, P.; Langer, G.; Müller, W. Homogenisieren strukturviskoser Flüssigkeiten in Schlaufenreaktoren und Rührkesseln. *Chem. Ing. Tech.* **1986**, *58*, 820–821. [[CrossRef](#)]
10. Warnecke, H.J.; Geisendörfer, M.; Hempel, D.C. Mass transfer behaviour of gas-liquid jet loop reactors. *Chem. Eng. Technol.-CET* **1988**, *11*, 306–311. [[CrossRef](#)]
11. Tebel, K.H.; Zehner, P. Fluid dynamic description of jet-loop reactors in multiphase operation. *Chem. Eng. Technol.-CET* **1989**, *12*, 274–280. [[CrossRef](#)]
12. Warnecke, H.J. Macromixing characteristics of gas-liquid jet loop reactors. *Acta Biotechnol.* **1989**, *9*, 111–121. [[CrossRef](#)]
13. Yagna Prasad, K.; Ramanujam, T. Enhancement of gas-liquid mass transfer in a modified reversed flow jet loop reactor with three-phase system. *Chem. Eng. Sci.* **1995**, *50*, 2997–3000. [[CrossRef](#)]
14. Jamshidi, A.M.; Sohrabi, M.; Vahabzadeh, F.; Bonakdarpour, B. Studies on the hydrodynamic behavior and mass transfer in a down-flow jet loop reactor with a coaxial draft tube. *J. Chem. Technol. Biotechnol.* **2001**, *76*, 39–46. [[CrossRef](#)]
15. Farizoglu, B.; Keskinler, B. Influence of draft tube cross-sectional geometry on  $K_L a$  and  $\epsilon$  in jet loop bioreactors (JLB). *Chem. Eng. J.* **2007**, *133*, 293–299. [[CrossRef](#)]
16. Behr, A.; Becker, M.; Dostal, J.; Kohlmann, D. Hydrodynamik und Verweilzeitverhalten eines Düsenumlaufreaktors für den Einsatz in der Mehrphasenkatalyse. *Chem. Ing. Tech.* **2008**, *80*, 1501–1508. [[CrossRef](#)]
17. Bey, O.; von Harbou, E. Einfluss der Wechselwirkung von Reaktion und Fluidodynamik auf das Verhalten von Strahlschlaufenreaktoren. *Chem. Ing. Tech.* **2021**, *93*, 191–200. [[CrossRef](#)]
18. Warmeling, H.; Behr, A.; Vorholt, A.J. Jet loop reactors as a versatile reactor set up—Intensifying catalytic reactions: A review. *Chem. Eng. Sci.* **2016**, *149*, 229–248. [[CrossRef](#)]
19. *DIN EN 13445-1:2018-12*; Unfired Pressure Vessels—Part 1: General. DIN Deutsches Institut für Normung e. V.: Berlin, Germany, 2018.
20. Kraume, M. *Transportvorgänge in der Verfahrenstechnik*, 3rd ed.; Springer: Berlin/Heidelberg, Germany, 2020. [[CrossRef](#)]
21. Wiedemann, M. *Einfluss der lokalen Energiedissipationsdichte in Reaktoren auf Umsatz und Selektivität chemischer Reaktionen*; Berichte aus der Verfahrenstechnik, Shaker: Aachen, Germany, 2011.
22. Dreimann, J.; Behr, A.; Vorholt, A.J. Reaktoren für Fluid-Fluid-Reaktionen: Strahldüsenreaktoren. In *Handbuch Chemische Reaktoren: Grundlagen und Anwendungen der Chemischen Reaktionstechnik*; Reschetilowski, W., Ed.; Springer: Berlin/Heidelberg, Germany, 2018; pp. 1–28. [[CrossRef](#)]
23. Aizad, S.; Yahaya, B.H.; Zubairi, S.I. Fabrication of 3-D polymeric scaffold: The development of continuous flow salt leaching kit coupled with ion conductivity detection. *Regen. Res.* **2014**, *3*, 165–168.
24. Stieß, M. *Mechanische Verfahrenstechnik-Partikeltechnologie 1*, 3rd ed.; Springer: Berlin/Heidelberg, Germany, 2009; pp. 34–37. [[CrossRef](#)]
25. Garcia-Ochoa, F.; Gomez, E. Bioreactor scale-up and oxygen transfer rate in microbial processes: An overview. *Biotechnol. Adv.* **2009**, *27*, 153–176. [[CrossRef](#)] [[PubMed](#)]
26. Rosseburg, A.; Fitschen, J.; Wutz, J.; Wucherpennig, T.; Schlüter, M. Hydrodynamic inhomogeneities in large scale stirred tanks—Influence on mixing time. *Chem. Eng. Sci.* **2018**, *188*, 208–220. [[CrossRef](#)]